SUPPORTING INFORMATION

Nonequivalence of Second Sphere "Noncatalytic" Residues in Pentaerythritol Tetranitrate Reductase in Relation to Local Dynamics Linked to H-Transfer in Reactions with NADH and NADPH Coenzymes

Andreea I. Iorgu[†], Nicola J. Baxter[†‡], Matthew J. Cliff[†], Colin Levy[†], Jonathan P. Waltho[†‡], Sam Hay[†], Nigel S. Scrutton[†]*

[†] Manchester Institute of Biotechnology and School of Chemistry, Faculty of Science and Engineering, The University of Manchester, 131 Princess Street, Manchester M1 7DN, United Kingdom

[‡] Krebs Institute for Biomolecular Research, Department of Molecular Biology and Biotechnology, The University of Sheffield, Firth Court, Western Bank, Sheffield S10 2TN, United Kingdom

*nigel.scrutton@manchester.ac.uk

TABLE OF CONTENTS

EXPERIMENTAL SECTION

Materials. All reagents were of analytical grade and were purchased from Sigma-Aldrich (Dorset, UK), except for NADP⁺, NADH and NADPH, which were obtained from Melford Laboratories (Chelsworth, U.K.). All isotopically enriched compounds (^2H_2O, $^{15}NH_4Cl$ and $^2H_7,^{13}C_6$-D-glucose) used for $^2H,^{13}C,^{15}N$-labeled PETNR overexpression were obtained from Goss Scientific Ltd. (Crewe, U.K.).

Preparation of deuterated and reduced coenzymes. (*R*)-[4-^2H]-NADPH and (*R*)-[4-^2H]-NADH were synthesized by enzymatic stereospecific reduction of NADP⁺ or NAD⁺ and purified as previously described (purity determination by ^1H NMR spectroscopy confirmed isotopic purity >98.5%).[1] NAD(P)H₄ was synthesized by reduction of NAD(P)H with hydrogen using palladium-activated charcoal, and isolated as described before.[1]

Overexpression and purification of variant enzymes. The desired mutations were introduced into the PETNR-containing pONR1 gene using the Stratagene QuikChange II Site-Directed Mutagenesis Kit (Stockport, UK), with custom primers ordered from Eurofins Genomics (Ebersberg, Germany). The correct mutations were confirmed by DNA sequencing (Eurofins Genomics), and the variant enzymes were overexpressed and purified as described before for WT enzyme.[2,3] $^2H,^{13}C,^{15}N$-labeled PETNR samples that were used in NMR experiments were prepared as previously described.[4]

Extinction coefficients. Enzyme concentrations were determined using the calculated molar extinction coefficients at 465 nm (see Table S1). NAD(P)H and (*R*)-[4-^2H]-NAD(P)H concentrations were determined using a molar extinction coefficient of 6.22 mM^{-1} cm^{-1} at 340 nm, while NAD(P)H₄ concentrations were determined using a molar extinction coefficient of 16.8 mM^{-1} cm^{-1} at 289 nm.[1]

Stopped-flow spectroscopy. All kinetic measurements were performed using a Hi-Tech Scientific (TgK Scientific, Bradford on Avon, U.K.) stopped-flow spectrophotometer, which had the sample handling unit placed inside a Belle Technology anaerobic glovebox (<5 ppm of O_2). All buffer solutions (50 mM potassium phosphate buffer, pH 7.0) used for the measurements were degassed by bubbling nitrogen gas through the solution for 1 hour prior to transfer to the glovebox, and were left overnight to equilibrate in the glovebox and ensure removal of all oxygen traces. All concentration dependence measurements were performed at 25 °C, using a constant (~20 µM) enzyme concentration throughout, and with varying NADPH or NADH concentrations (0.1 – 20 mM and 0.3-50 mM final concentration, respectively). Temperature dependence measurements were performed using a constant enzyme concentration (20 µM) and a constant concentration of NADPH and NADH (10 mM and 25 mM final concentration, respectively), in order to ensure pseudo-first order kinetics for all variants throughout the whole temperature range (5-40 °C). All absorption traces were analyzed and fitted with standard exponential decay functions, using OriginPro 9.1 (OriginLab Corporation, MA, USA). The reported observed rate constants represent the mean average of 3-6 individual measurements, and the error bars are plotted as ± 1 standard deviation.

Crystallography. The crystallization conditions used were similar to those previously reported.[3] Sitting drop vapor diffusion was used to obtain crystals by mixing 200 nl of 15 mg/ml protein (20 mM Tris/HCl, pH 8.0 at 4 °C) with 400 nl of a reservoir containing 25 % (w/v) PEG 3000, 17 % (v/v) isopropanol, 0.1 M trisodium citrate, 0.1 M cacodylic acid (pH 6.5). Plates were incubated at 21 °C and crystal formation was observed after 48 hours. Individual crystals were harvested and cryo-cooled by plunging into liquid nitrogen prior to data collection at Diamond Light Source. Single cryo-cooled crystals of each of the four PETNR variants were used to collect complete data sets, which were subsequently scaled and integrated using Xia2.[5] Structures were solved by molecular replacement in Phaser[6] using a search model derived from the wild type PETNR structure

(3P62). Iterative cycles of model building and refinement were performed using COOT and Phenix.[7,8] Validation with MOLPROBITY[9] and PDB-REDO[10] was integrated into the iterative rebuilding and refinement process. Complete data collection and refinement statistics are presented in Table S1.

NMR spectroscopy. Sequential backbone assignment of the PETNR−NAD(P)H$_4$ complexes was performed using an enzyme:ligand ratio of 1:10, to ensure the presence of a high population of saturated complex (K_d values for the PETNR−NADPH$_4$ and PETNR−NADH$_4$ complexes are 0.13 mM and 0.14 mM, respectively).[11] As the coenzyme analogues have a limited stability, as previously observed for the NAD(P)H coenzymes, the samples were prepared just prior to NMR spectral acquisition. All NMR experiments were conducted under identical conditions to those recently reported for the PETNR holoenzyme.[4] In summary, samples of approximately 1 mM ^{2}H,^{13}C,^{15}N-labeled PETNR, in 50 mM potassium phosphate buffer, pH 7.0, supplemented with 1 mM NaN$_3$ and containing 10 mM NAD(P)H$_4$ coenzyme analogue were used. All samples contained 10% (v/v) ^{2}H$_2$O, added as an internal lock, and 0.5% (v/v) trimethylsilyl propanoic acid (TSP), used for chemical shift referencing. ^{1}H chemical shifts were referenced relative to the internal TSP signal, whereas ^{15}N and ^{13}C chemical shifts were indirectly referenced using the nuclei-specific gyromagnetic ratios.[12] NMR experiments were recorded at 298 K on an 800 MHz Bruker Avance III spectrometer (Bruker Corp., U.S.A.), equipped with a 5 mm ^{1}H/^{13}C/^{15}N TCI cryoprobe and a Z-field gradient coil, running Topspin v.3.2 (Bruker Corp., U.S.A.). The backbone assignment of the PETNR−NAD(P)H$_4$ complexes was achieved using ^{1}H-^{15}N TROSY HSQC and TROSY versions of HNCACB, HN(CO)CACB, HNCA, HN(CA)CO and HNCO triple resonance experiments.[13] NMR data were processed using Topspin v.3.2 software and analyzed using CCpNmr Analysis v.2.4 software.[14] The chemical shift assignments for PETNR−NADPH$_4$ and PETNR−NADH$_4$ complexes have been deposited in the Biological Magnetic Resonance Bank (BMRB: http://www.bmrb.wisc.edu/) under the accession numbers 27469 and 27470, respectively.

STATIC UV-VIS SPECTROSCOPY DATA
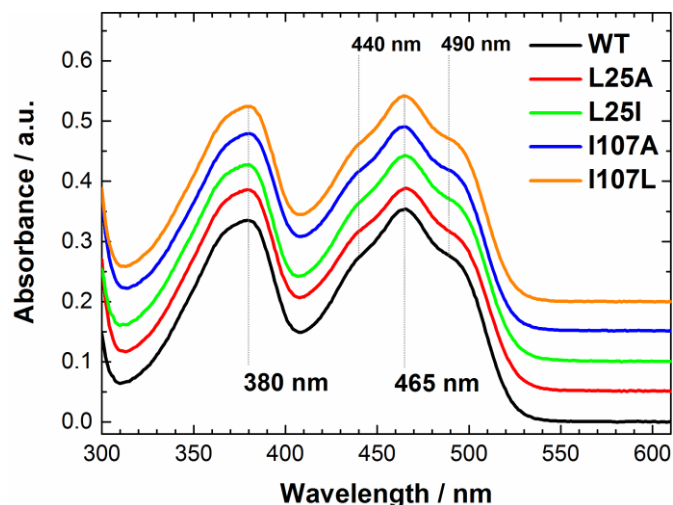
Figure S1. UV-vis absorption spectra of the PETNR variants. The broad absorbance peaks at 380 nm and 465 nm are characteristic of the oxidized form of PETNR-bound FMN, and it can be noted there are no observable changes in the shape of the spectra upon mutagenesis. For a better comparison, all spectra are vertically shifted, with the absorbance scale correlated with the WT PETNR data. Conditions: 30 μM enzyme, 50 mM potassium phosphate buffer (pH 7.0), 25 °C.

Table S1. Determination of Flavin Stoichiometry and Calculated Extinction Coefficients at 465 nm for the PETNR variants.

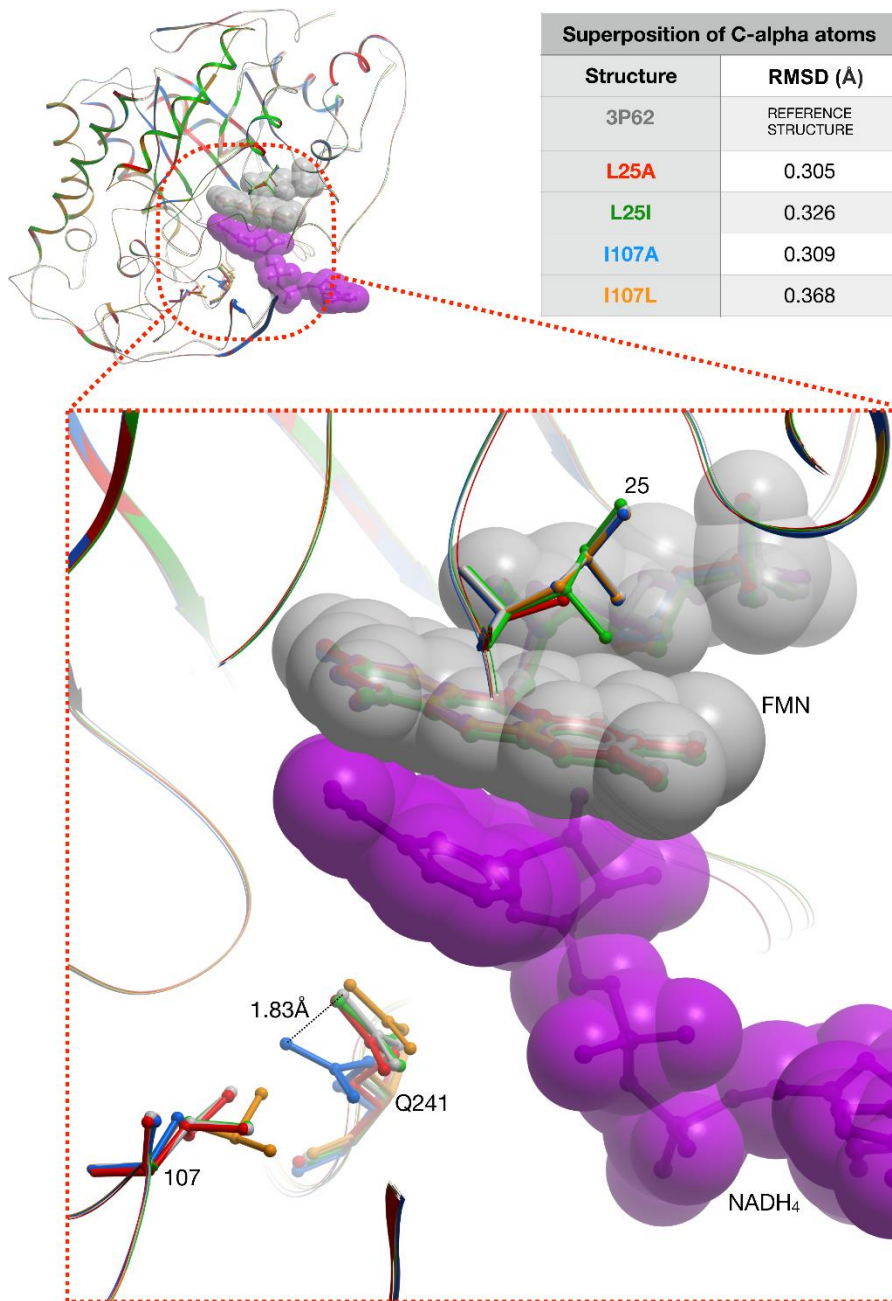| PETNR variant	[Apoenzyme][a] mg/mL	[Apoenzyme] μM	A_{445nm}[b] a.u.	[FMN][c] μM	[FMN]:[Apoenzyme][d]	A_{465nm}[e]	ε_{465nm}[f] $cm^{-1}\ mM^{-1}$
WT	0.98	24.4	0.30	23.9	0.98	0.27	11.25
L25A	0.72	17.9	0.22	17.2	0.96	0.20	11.34
L25I	0.64	16.1	0.19	15.3	0.95	0.18	11.52
I107A	0.73	18.3	0.23	18.7	1.02	0.21	11.22
I107L	0.93	23.2	0.28	22.2	0.96	0.25	11.33

[a]apoenzyme concentration calculated using the DC Protein Assay from Bio-Rad Laboratories Ltd. (Hertfordshire, U.K.); [b]absorbance of free flavin measured after protein denaturation (the protein stock solution was denatured by incubation at 95 °C for 10 min in the dark, and the denatured protein was removed by centrifugation at 13,000 rpm for 10 min in a micro centrifuge); [c]calculated using the extinction coefficient of free FMN in solution (12.5 $cm^{-1}\ mM^{-1}$); [d]stoichiometry of samples (% of bound flavin) - we estimate an error of ± 5% on these values; [e]absorbance at 465 nm for each variant (FMN-bound PETNR); [f]extinction coefficient of each variant; the same protein stocks (with concentrations between 15-30 μM) were used for all measurements presented herein.
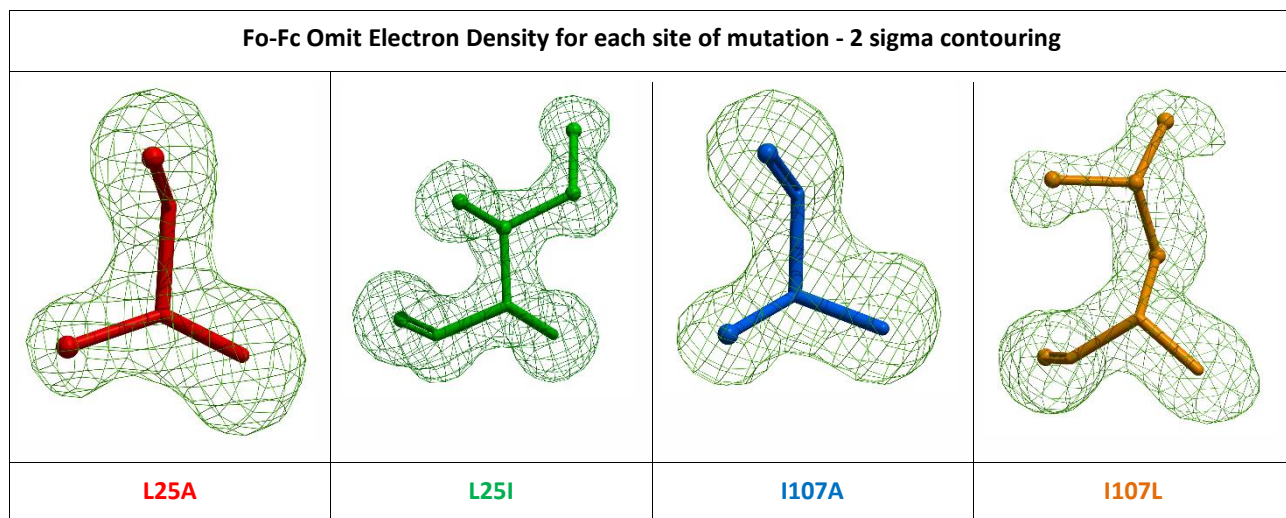
The results presented in Table S1 indicate that all PETNR variants present essentially 1:1 stoichiometry between the FMN cofactor and the apoenzyme (determined ratios between 0.96-1.02), and also the same value of the extinction coefficient at 465 nm (~ 11.3 $cm^{-1}\ mM^{-1}$ for all variants).

CRYSTALLOGRAPHY DATA

Table S2. Data Collection Statistics for the Crystal Structures of Investigated PETNR Variants.

	L25A (PDB: 6GI8)	L25I (PDB: 6GI7)	I107A (PDB: 6GIA)	I107L (PDB: 6GI9)
Wavelength	0.9763	0.92	0.92	0.9686
Resolution range	54.44 - 1.42	48.5 - 1.3	37.39 - 1.7	37.54 - 1.45
	(1.471 - 1.42)	(1.346 - 1.3)	(1.761 - 1.7)	(1.502 - 1.45)
Space group	P 21 21 21	P 21 21 21	P 21 21 21	P 21 21 21
Unit cell	56.808 68.875 88.874	57.76 70.53 89.31	56.8716 69.1394	57.32 70.32 88.78
	90 90 90	90 90 90	88.8937 90 90 90	90 90 90
Total reflections	532239 (52383)	1623254 (156692)	134933 (13196)	227721 (22053)
Unique reflections	66485 (6534)	89476 (8544)	39076 (3865)	63458 (6292)
Multiplicity	8.0 (8.0)	18.1 (18.3)	3.5 (3.4)	3.6 (3.5)
Completeness (%)	99.97 (99.98)	98.93 (95.65)	99.39 (99.41)	98.68 (99.31)
Mean I/sigma(I)	15.88 (2.16)	22.94 (9.68)	14.92 (3.54)	13.19 (2.16)
Wilson B-factor	14.71	7.32	16.27	13.03
R-merge	0.08077 (0.917)	0.08843 (0.2971)	0.05966 (0.4119)	0.06332 (0.6041)
R-meas	0.08634 (0.9803)	0.09105 (0.3054)	0.07095 (0.4883)	0.07426 (0.7131)
R-pim	0.03014 (0.3435)	0.02141 (0.0697)	0.03781 (0.2585)	0.03787 (0.3706)
CC1/2	0.999 (0.682)	0.998 (0.985)	0.99 (0.778)	0.998 (0.728)
CC*	1 (0.9)	1 (0.996)	0.997 (0.936)	1 (0.918)
Reflections used in re-finement	66464 (6534)	89319 (8544)	39050 (3861)	63456 (6292)
Reflections used for R-free	3377 (330)	4545 (446)	1919 (194)	3221 (334)
R-work	0.1323 (0.1969)	0.1108 (0.0947)	0.1453 (0.1571)	0.1248 (0.2076)
R-free	0.1798 (0.2504)	0.1396 (0.1351)	0.2033 (0.2581)	0.1641 (0.2616)
CC(work)	0.968 (0.903)	0.972 (0.976)	0.970 (0.934)	0.973 (0.909)
CC(free)	0.961 (0.797)	0.965 (0.961)	0.935 (0.839)	0.968 (0.872)
Number of non-hydro-gen atoms	3409	3751	3240	3393
macromolecules	2855	3035	2818	2850
ligands	35	35	35	35
solvent	519	681	387	508
Protein residues	363	362	362	363
RMS(bonds)	0.016	0.012	0.009	0.013
RMS(angles)	1.62	1.56	1.32	1.52
Ramachandran favored (%)	97.22	97.22	96.39	98.06
Ramachandran al-lowed (%)	2.78	2.78	3.61	1.94
Ramachandran outliers (%)	0	0	0	0
Rotamer outliers (%)	1.02	0.64	0.69	1.36
Clashscore	2.45	5.26	1.06	1.4
Average B-factor	19.19	10.56	19.74	16.68
macromolecules	16.95	8.09	18.68	14.25
ligands	12.34	6.21	14.62	10.44
solvent	31.96	21.81	27.93	30.75

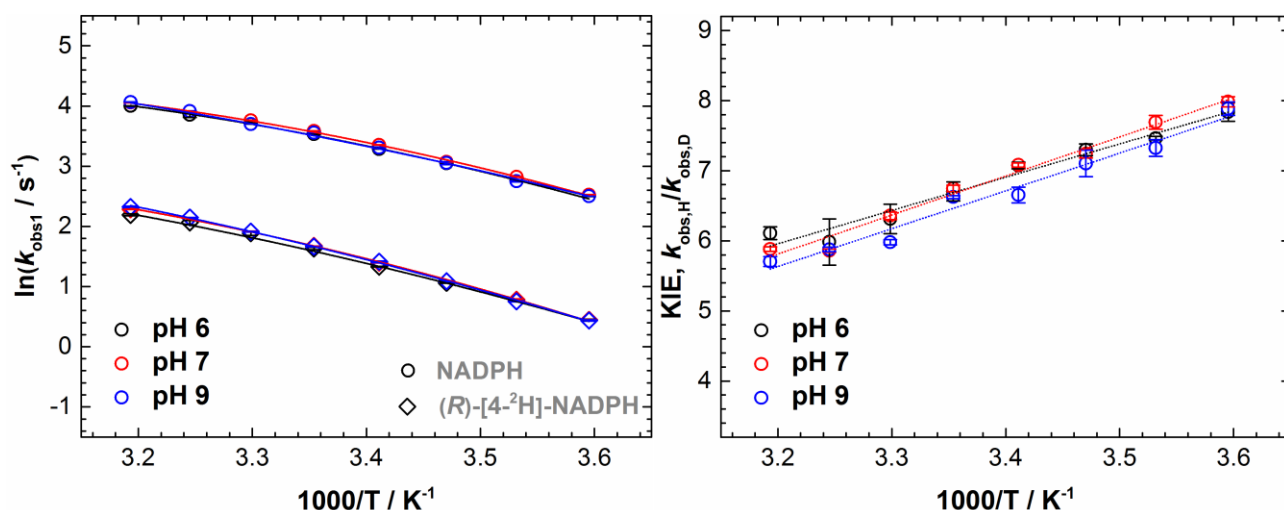| Superposition of C-alpha atoms	
Structure	RMSD (Å)
3P62	REFERENCE STRUCTURE
L25A	0.305
L25I	0.326
I107A	0.309
I107L	0.368

Figure S2. X-ray crystal structures of investigated PETNR variants. Each of the four variant PETNR crystal structures has been superimposed onto the WT PETNR structure (PDB: 3P62), and the C-alpha RMSD values are presented in the top right table. The C-alpha traces for each of the five structures are shown top left, colored according to the convention adopted throughout this manuscript. To highlight the coenzyme binding region, the PETNR–NADH$_4$ complex structure (PDB: 3KFT) was also super-imposed onto the WT structure (3P62) and NADH$_4$ from this structure is shown in purple CPK representation. The sites of mutation along with residue Q241 are shown in ball and stick representation. The side chain of Q241 has moved ~1.83Å relative to the position observed in the wild type structure for the I107A variant. Movement at Q241 will influence the spatial freedom available to the nicotinamide coenzyme. All variant structures show an alternative primary conformation at C5 of the FMN cofactor compared to that observed in WT PETNR. However, despite this variability, the hydrogen bonding networks of the FMN are maintained and consistent with those in WT PETNR.

Fo-Fc Omit Electron Density for each site of mutation - 2 sigma contouring			
L25A	**L25I**	**I107A**	**I107L**

Figure S3. Electron density for each site of mutation in PETNR. Each of the four mutations are displayed in ball and stick representation and colored according to the convention adopted throughout the manuscript.
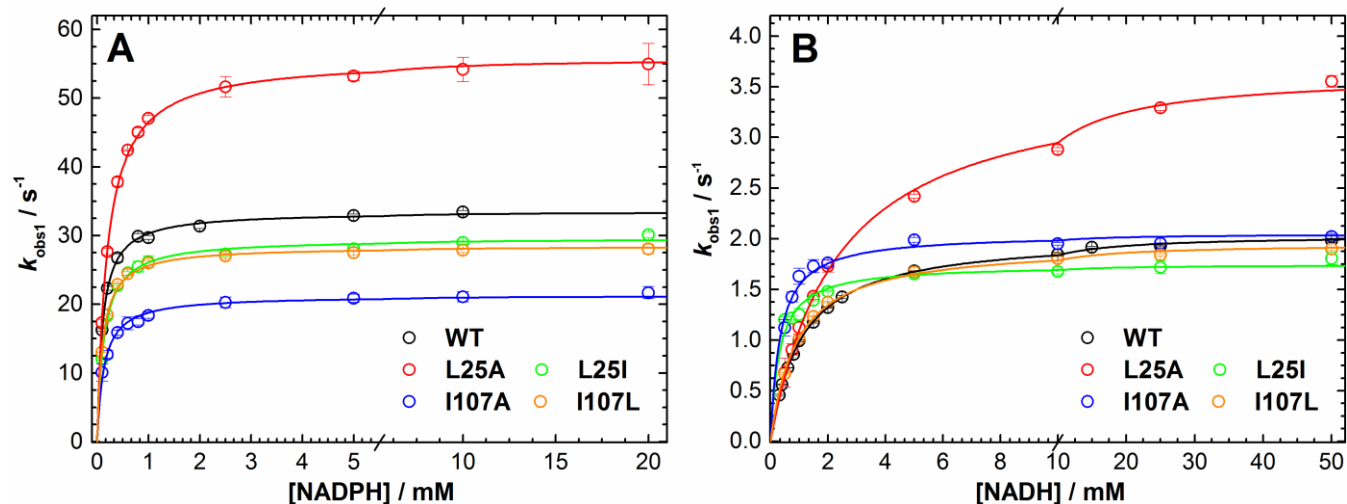
Figure S4. Temperature dependence of the observed rate constants (k_{obs}) of FMN Reduction for WT PETNR with NADPH and (R)-[4-^{2}H]-NADPH at pH 6, pH 7 and pH9 (A) and the corresponding temperature dependencies of the observed primary kinetic isotope effects (B). The measurements were performed in MTEN buffer (50 mM MES, 25 mM Tris, 25 mM ethanolamine, and 100 mM NaCl), which has a useful buffering capacity and minimal change in ionic strength over the pH range 6-9 in which PETNR is stable; we attempted testing PETNR in pH 5 as well, but the enzyme is unstable at this pH. The observed rate constants of FMN reduction at pH 7 in MTEN buffer are essentially the same to those measured in 50 mM potassium phosphate buffer, pH 7 and similar observation are valid for the KIEs values (Table S3).The rate of FMN reduction is essentially insensitive to pH across the whole temperature range (5-40 °C), and also that KIEs values are essentially not affected by changes in pH (the rate of FMN reduction by (R)-[4-^{2}H]-NADPH is independent of pH as well across all temperatures studied; see Table S3 for extracted thermodynamic parameters). Although these experiments cannot completely exclude any kinetic complexity, they clearly indicate that at least the observed rates of FMN reduction do not reflect on a concerted mechanism of H-transfer and protonation (which would lead to pH-dependent rates) which makes it very likely that the observed rate are reporting directly on the H-transfer step.

Table S3. Extracted Thermodynamic Parameters from pH Dependence Studies.

	$\Delta H_{T0}^{\ddagger}$ (kJ mol^{-1})	$\Delta S_{T0}^{\ddagger}$ (J mol^{-1} K^{-1})	$\Delta C_p^{\ddagger}$ (kJ mol^{-1} K^{-1})
	NADPH		
pH 6	27.2 ± 0.6	-124.3 ± 2.0	-0.58 ± 0.10
pH 7	27.6 ± 0.7	-122.7 ± 1.6	-0.61 ± 0.08
pH 9	28.9 ± 0.7	-118.6 ± 2.3	-0.45 ± 0.12
	(R)-[4-^{2}H]-NADPH		
pH 6	33.0 ± 0.9	-120.6. ± 2.9	-0.57 ± 0.15
pH 7	34.6 ± 0.5	-115.0 ± 1.8	-0.54 ± 0.09
pH 9	35.5 ± 0.4	-111.9 ± 1.3	-0.48 ± 0.07
	Isotope effect: (R)-[4-^{2}H]-NADPH - NADPH		
pH 6	5.8 ± 1.1	3.7 ± 3.5	0.01 ± 0.18
pH 7	7.0 ± 0.7	7.7 ± 2.4	0.07 ± 0.12
pH 9	6.6 ± 0.8	6.7 ± 2.6	-0.03 ± 0.13

Figure S5. Concentration dependence of FMN reduction in the PETNR variants with NADPH (A) and NADH (B), recorded at 25 °C. Conditions: 50 mM potassium phosphate buffer (pH 7.0), 20 μM enzyme and varying coenzyme concentrations. In the cases where the reaction is multiphasic, only the fast observed rate constants (k_{obs1}) are represented and fitted. *Note:* For the variants exhibiting multiphasic behavior at 25 °C (see below in Tables S2-S11), the slow observed rate constants (k_{obs2}) have constant values and amplitudes (within error) throughout the range of NAD(P)H concentrations studied, suggesting the K_s for k_{obs2} is very low (<10 μM). This observation ensures that further (i.e. temperature dependence) experiments are recorded under saturating conditions for all kinetic phases observed.

TABULATED RATE CONSTANTS FROM TEMPERATURE DEPENDENCE STUDIES

Table S4. Temperature Dependence of the Observed Rate Constants (k_{obs}) of FMN Reduction for WT PETNR with NADPH and (R)-[4-^{2}H]-NADPH.

T (°C)	NADPH			(R)-[4-^{2}H]-NADPH		
	k_{obs1} (s^{-1})	k_{obs2} (s^{-1})	A$_2$* (%)	k_{obs1} (s^{-1})	k_{obs2} (s^{-1})	A$_2$ (%)
5	11.31 ± 0.09	-	-	1.51 ± 0.01	-	-
10	15.23 ± 0.15	-	-	2.13 ± 0.01	-	-
15	20.32 ± 0.25	-	-	2.90 ± 0.01	-	-
20	26.28 ± 0.31	-	-	3.95 ± 0.02	-	-
25	33.74 ± 0.46	-	-	5.20 ± 0.04	-	-
30	41.64 ± 0.20	-	-	6.59 ± 0.04	-	-
35	50.46 ± 0.75	1.19 ± 0.92	1.41 ± 0.23	8.48 ± 0.03	1.22 ± 0.45	2.54 ± 0.53
40	58.49 ± 0.50	1.09 ± 0.16	2.29 ± 0.35	9.96 ± 0.18	1.11 ± 0.24	3.41 ± 0.65

*A$_2$ represents the change in amplitude corresponding to k_{obs2}, out of the total change in absorbance (A$_{464nm}$).

Table S5. Temperature Dependence of the Observed Rate Constants (k_{obs}) of FMN Reduction for L25A PETNR with NADPH and (R)-[4-^{2}H]-NADPH.

T (°C)	NADPH			(R)-[4-^{2}H]-NADPH		
	k_{obs1} (s^{-1})	k_{obs2} (s^{-1})	A$_2$ (%)	k_{obs1} (s^{-1})	k_{obs2} (s^{-1})	A$_2$ (%)
5	19.18 ± 0.22	0.65 ± 0.215	2.93 ± 0.55	2.37 ± 0.01	-	-
10	26.03 ± 0.17	1.85 ± 0.64	2.70 ± 0.56	3.33 ± 0.03	-	-
15	34.93 ± 1.25	3.75 ± 3.25	4.36 ± 2.77	4.59 ± 0.03	-	-
20	43.51 ± 0.64	2.42 ± 0.48	3.58 ± 0.47	6.14 ± 0.04	-	-
25	53.77 ± 1.15	1.54 ± 0.45	4.73 ± 0.26	8.01 ± 0.22	0.03 ± 0.03	8.80 ± 4.08
30	59.63 ± 2.29	0.64 ± 1.50	7.50 ± 0.21	10.24 ± 0.05	0.16 ± 0.03	5.83 ± 0.60
35	68.39 ± 8.69	0.51 ± 0.17	16.48 ± 0.53	11.89 ± 0.07	0.17 ± 0.01	14.06 ± 0.45
40*	71.16 ± 6.56	0.26 ± 0.06	25.54 ± 0.91	12.39 ± 0.22	0.26 ± 0.02	31.19 ± 1.07

*A third phase is observed at 40 °C for the reaction with NADPH with k_{obs3} of 3.55 ± 1.03 and A$_3$ = 19.34 ± 0.54.

Table S6. Temperature Dependence of the Observed Rate Constants (k_{obs}) of FMN Reduction for L25I PETNR with NADPH and (R)-[4-^{2}H]-NADPH.

T (°C)	NADPH			(R)-[4-^{2}H]-NADPH		
	k_{obs1} (s^{-1})	k_{obs2} (s^{-1})	A$_2$ (%)	k_{obs1} (s^{-1})	k_{obs2} (s^{-1})	A$_2$ (%)
5	10.12 ± 0.04	-	-	1.26 ± 0.02	-	-
10	13.47 ± 0.06	-	-	1.79 ± 0.01	-	-
15	18.07 ± 0.05	-	-	2.46 ± 0.01	-	-
20	24.33 ± 0.52	2.25 ± 2.63	3.28 ± 1.62	3.42 ± 0.03	0.19 ± 0.04	2.63 ± 0.15
25	30.24 ± 0.42	3.74 ± 1.20	3.96 ± 0.87	4.50 ± 0.02	0.27 ± 0.03	3.59 ± 0.27
30	36.74 ± 0.28	2.57 ± 0.62	4.00 ± 0.57	5.72 ± 0.06	0.28 ± 0.01	4.31 ± 0.37
35	43.84 ± 0.36	1.99 ± 0.12	5.72 ± 0.36	7.20 ± 0.07	0.42 ± 0.07	7.05 ± 0.36
40	49.82 ± 1.14	2.06 ± 0.19	10.89 ± 0.63	8.66 ± 0.09	0.66 ± 0.01	12.46 ± 0.45

Table S7. Temperature Dependence of the Observed Rate Constants (k_{obs}) of FMN Reduction for I107A PETNR with NADPH and (R)-[4-2H]-NADPH.

	NADPH			(R)-[4-^{2}H]-NADPH		
T (°C)	k_{obs1} (s^{-1})	k_{obs2} (s^{-1})	A$_2$ (%)	k_{obs1} (s^{-1})	k_{obs2} (s^{-1})	A$_2$ (%)
5	8.45 ± 0.08	1.46 ± 0.12	6.12 ± 0.67	1.01 ± 0.01	-	-
10	11.05 ± 0.13	2.60 ± 0.28	7.02 ± 0.79	1.43 ± 0.03	0.42 ± 0.26	4.21 ± 2.11
15	14.31 ± 0.34	3.29 ± 0.54	9.94 ± 2.01	1.90 ± 0.02	0.42 ± 0.16	3.81 ± 1.16
20	17.69 ± 0.14	3.29 ± 0.18	12.53 ± 0.12	2.39 ± 0.01	0.33 ± 0.05	3.56 ± 0.33
25	22.08 ± 0.55	4.31 ± 0.18	22.89 ± 1.963	2.87 ± 0.04	0.24 ± 0.03	5.16 ± 0.27
30	22.75 ± 0.34	3.90 ± 0.107	32.66 ± 0.61	3.19 ± 0.02	0.28 ± 0.03	8.70 ± 0.69
35	18.23 ± 0.58	3.57 ± 0.20	38.27 ± 1.59	3.31 ± 0.02	0.38 ± 0.01	15.07 ± 0.95
40	12.15 ± 0.43	2.42 ± 0.18	32.08 ± 1.75	3.08 ± 0.1	0.46 ± 0.10	20.99 ± 0.65

Table S8. Temperature Dependence of the Observed Rate Constants (k_{obs}) of FMN Reduction for I107L PETNR with NADPH and (R)-[4-^{2}H]-NADPH.

	NADPH			(R)-[4-^{2}H]-NADPH		
T (°C)	k_{obs1} (s^{-1})	k_{obs2} (s^{-1})	A$_2$ (%)	k_{obs1} (s^{-1})	k_{obs2} (s^{-1})	A$_2$ (%)
5	9.05 ± 0.07	-	-	1.23 ± 0.03	-	-
10	12.34 ± 0.156	-	-	1.74 ± 0.01	-	-
15	16.65 ± 0.21	-	-	2.42 ± 0.01	-	-
20	21.84 ± 0.34	-	-	3.31 ± 0.02	-	-
25	27.36 ± 0.40	-	-	4.37 ± 0.02	-	-
30	33.87 ± 0.50	-	-	5.52 ± 0.04	-	-
35	43.71 ± 1.29	4.22 ± 1.79	6.81 ± 1.84	7.05 ± 0.13	1.05 ± 0.26	4.43 ± 1.03
40	47.70 ± 2.88	3.37 ± 0.90	12.22 ± 2.91	8.14 ± 0.12	1.19 ± 0.10	10.87 ± 0.74

Table S9. Temperature Dependence of the Observed Rate Constants (k_{obs}) of FMN Reduction for WT PETNR with NADH and (R)-[4-^{2}H]-NADH.

	NADH			(R)-[4-^{2}H]-NADH		
T (°C)	k_{obs1} (s^{-1})	k_{obs2} (s^{-1})	A$_2$ (%)	k_{obs1} (s^{-1})	k_{obs2} (s^{-1})	A$_2$ (%)
5	0.73 ± 0.01	-	-	0.091 ± 0.001	-	-
10	0.92 ± 0.01	-	-	0.119 ± 0.001	-	-
15	1.17 ± 0.01	-	-	0.156 ± 0.001	-	-
20	1.51 ± 0.01	-	-	0.204 ± 0.002	-	-
25	1.95 ± 0.01	-	-	0.274 ± 0.001	-	-
30	2.53 ± 0.02	-	-	0.366 ± 0.002	-	-
35	3.30 ± 0.01	-	-	0.499 ± 0.011	-	-
40	4.25 ± 0.02	-	-	0.673 ± 0.005	-	-

Table S10. Temperature Dependence of the Observed Rate Constants (k_{obs}) of FMN Reduction for L25A PETNR with NADH and (R)-[4-^{2}H]-NADH.

	NADH			(R)-[4-^{2}H]-NADH		
T (°C)	k_{obs1} (s^{-1})	k_{obs2} (s^{-1})	A$_2$ (%)	k_{obs1} (s^{-1})	k_{obs2} (s^{-1})	A$_2$ (%)
5	1.27 ± 0.01	-	-	0.162 ± 0.002	-	-
10	1.61 ± 0.01	-	-	0.211 ± 0.002	-	-
15	2.03 ± 0.01	-	-	0.275 ± 0.004	-	-
20	2.63 ± 0.03	-	-	0.360 ± 0.004	-	-
25	3.33 ± 0.07	0.09 ± 0.06	2.29 ± 0.92	0.495 ± 0.002	-	-
30	4.23 ± 0.06	0.08 ± 0.01	4.93 ± 0.85	0.612 ± 0.042	-	-
35	5.20 ± 0.11	0.11 ± 0.01	12.72 ± 0.74	0.885 ± 0.018	0.11 ± 0.03	15.60 ± 2.69
40*	6.74 ± 0.37	0.13 ± 0.01	20.40 ± 1.48	1.070 ± 0.054	0.17 ± 0.01	34.60 ± 0.91

*A third phase is observed at 40 °C for the reaction with NADH with k_{obs3} of 1.10 ± 0.0 and a %A of 19.01 ± 3.17.

Table S11. Temperature Dependence of the Observed Rate Constants (k_{obs}) of FMN Reduction for L25I PETNR with NADH and (R)-[4-^{2}H]-NADH.

|	NADH			(R)-[4-^{2}H]-NADH		
T (°C)	k_{obs1} (s^{-1})	k_{obs2} (s^{-1})	A$_2$ (%)	k_{obs1} (s^{-1})	k_{obs2} (s^{-1})	A$_2$ (%)
5	0.49 ± 0.01	-	-	0.062 ± 0.001	-	-
10	0.66 ± 0.01	-	-	0.083 ± 0.001	-	-
15	0.90 ± 0.01	-	-	0.113 ± 0.002	-	-
20	1.20 ± 0.01	-	-	0.160 ± 0.001	-	-
25	1.77 ± 0.06	0.36 ± 0.10	6.40 ± 2.07	0.223 ± 0.003	-	-
30	2.39 ± 0.06	0.39 ± 0.09	6.86 ± 1.61	0.306± 0.005	-	-
35	3.26 ± 0.07	0.49 ± 0.07	8.92 ± 1.01	0.418 ± 0.001	-	-
40	4.26 ± 0.13	0.58 ± 0.05	12.28 ± 1.93	0.604± 0.066	-	-

Table S12. Temperature Dependence of the Observed Rate Constants (k_{obs}) of FMN Reduction for I107A PETNR with NADH and (R)-[4-^{2}H]-NADH.

	NADH			(R)-[4-^{2}H]-NADH		
T (°C)	k_{obs1} (s^{-1})	k_{obs2} (s^{-1})	A$_2$ (%)	k_{obs1} (s^{-1})	k_{obs2} (s^{-1})	A$_2$ (%)
5	0.42 ± 0.01	-	-	0.053 ± 0.001	-	-
10	0.62 ± 0.01	-	-	0.075 ± 0.003	-	-
15	0.92 ± 0.01	-	-	0.115 ± 0.001	-	-
20	1.35 ± 0.01	-	-	0.172 ± 0.005	-	-
25	1.97 ± 0.02	-	-	0.261 ± 0.007	-	-
30	2.75 ± 0.02	-	-	0.391 ± 0.004	-	-
35	3.63 ± 0.01	-	-	0.545 ± 0.008	-	-
40	4.29 ± 0.03	-	-	0.673± 0.013	-	-

Table S13. Temperature Dependence of the Observed Rate Constants (k_{obs}) of FMN Reduction for I107L PETNR with NADH and (R)-[4-^{2}H]-NADH.

	NADH			(R)-[4-^{2}H]-NADH		
T (°C)	k_{obs1} (s^{-1})	k_{obs2} (s^{-1})	A$_2$ (%)	k_{obs1} (s^{-1})	k_{obs2} (s^{-1})	A$_2$ (%)
5	0.61 ± 0.01	-	-	0.073 ± 0.003	-	-
10	0.81 ± 0.01	-	-	0.102 ± 0.002	-	-
15	1.06 ± 0.01	-	-	0.136 ± 0.003	-	-
20	1.40 ± 0.01	-	-	0.185 ± 0.004	-	-
25	1.87 ± 0.01	-	-	0.263 ± 0.003	-	-
30	2.49 ± 0.01	-	-	0.357 ± 0.010	-	-
35	3.30 ± 0.03	-	-	0.504 ± 0.001	-	-
40	4.25 ± 0.02	-	-	0.685± 0.019	-	-

ADDITIONAL KINETIC ANALYSIS
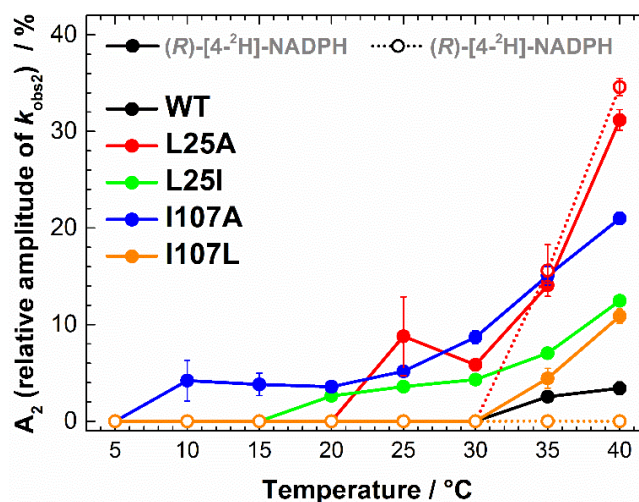
Figure S6. Manifestation of multiple reactive configurations as a function of temperature for the PETNR variants during FMN reduction with (R)-[4-^{2}H]-NADPH and (R)-[4-^{2}H]-NADH. For the variants exhibiting multiple reactive configurations, A$_2$ (the amplitude of slow observed rate, k_{obs2}) is increasing with increasing temperature, in the same manner as for the reduction of the variants with non-deuterated coenzymes.
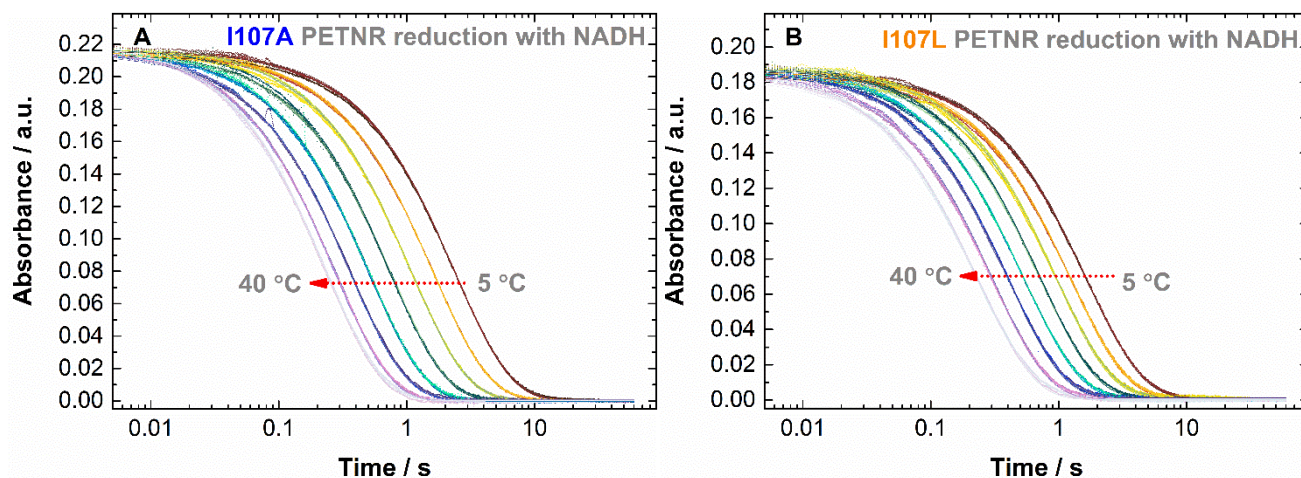
Figure S7. Raw kinetic transients showing the temperature dependence of the reduction of I107A (A) and I107L (B) with NADH coenzyme. The transients are represented as a scatter plot, with single exponential fitting functions depicted as thin lines of the same color. Note that all transients fit to single exponential decay functions across the temperature range studied, and the total change in absorbance is constant, eliminating the possibility of other secondary reactive (or unreactive) species (this would lead to a decrease in the total change with increasing temperature, as the amplitude of the second phase would increase, which is not the case herein).
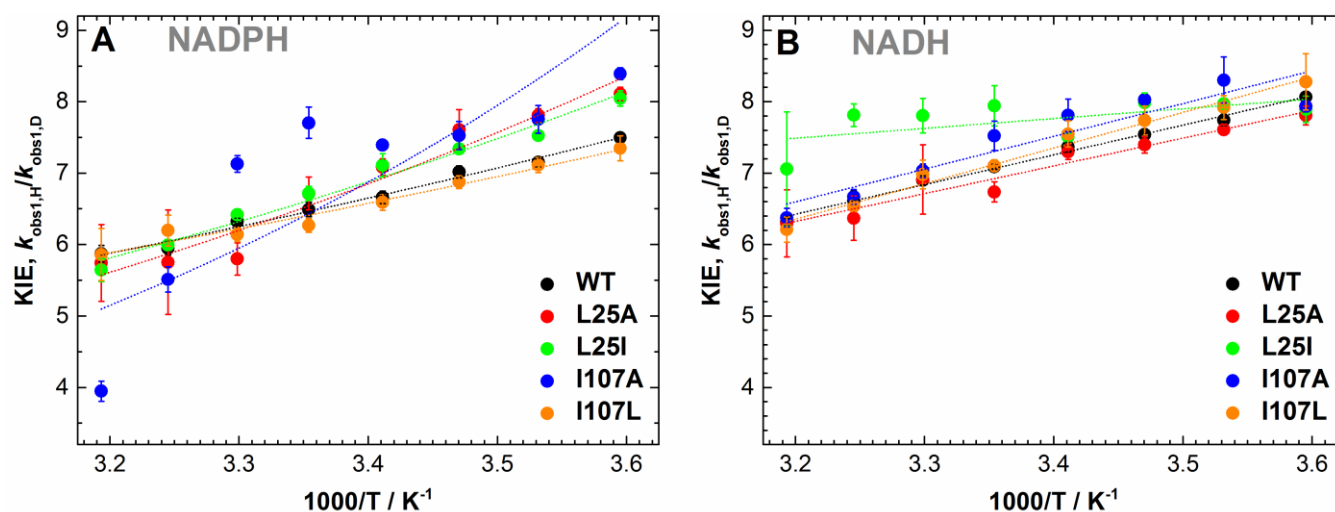
Figure S8. Temperature dependence of the observed primary kinetic isotope effects (KIEs) for FMN reduction in the PETNR variants with NADPH (A) and NADH (B). The solid lines are linear fits of each data set (for visual guidance). *Note:* The values presented in the current figure correspond to the KIE on the fast observed rate, k_{obs1}. See Figure S9 for KIEs on the slow observed rate, k_{obs2}.
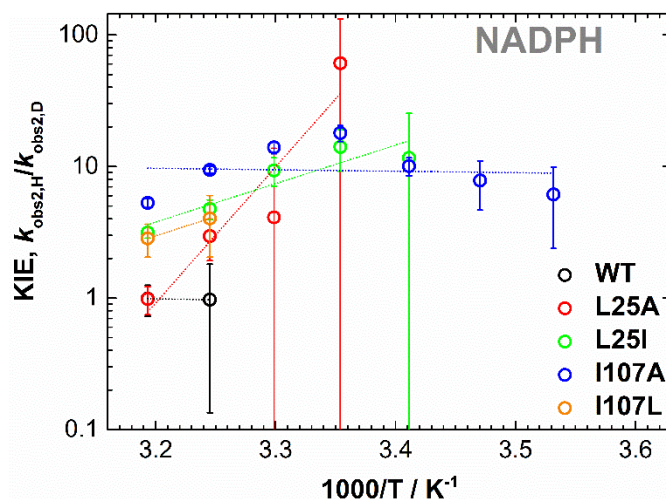
Figure S9. Temperature dependence of the KIEs for the slow observed rate (k_{obs2}) of FMN reduction in the PETNR variants with NADPH. The solid lines are linear fits of each data set (for visual guidance). While the presence of KIEs on k_{obs2} confirms (among other things) that the reduction of the enzyme occurs through different reactive configurations, with the multiphasic FMN reduction representing parallel pathways for H-transfer, the KIEs for k_{obs2} are not analyzed further, as the interpretation is limited by the small amplitudes and low values for k_{obs2}, which give rise to very high errors. *Note (for NADH reactions):* Although during the reactions with (R)-[4-^{2}H]-NADH it is expected to observe multiple phases, fitting could only be typically done using single exponential functions, and no KIEs could be extracted. This is expected, as the second phases for the deuterated coenzyme would probably have rate constants < 0.05 s^{-1}.
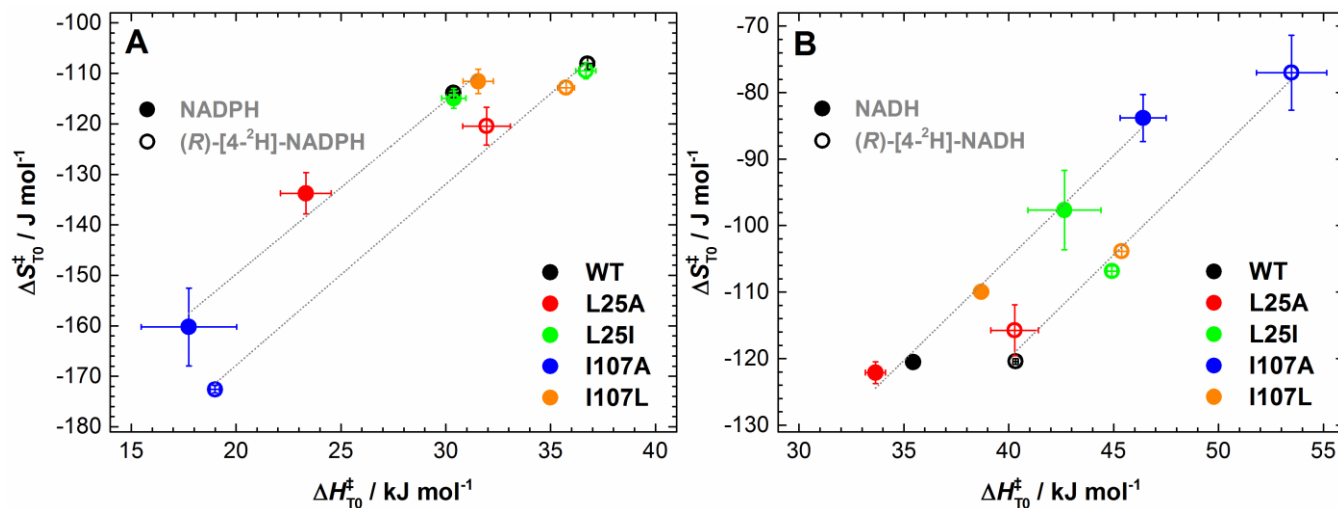

Figure S10. A) Relationship between the apparent activation enthalpy and entropy values determined for the reactions of NADPH and (R)-[4-^{2}H]-NADPH with the PETNR variants. The solid lines are linear fits of each data set to guide the eye. B) The same relationship illustrated for the reactions with NADH and (R)-[4-^{2}H]-NADH coenzymes.
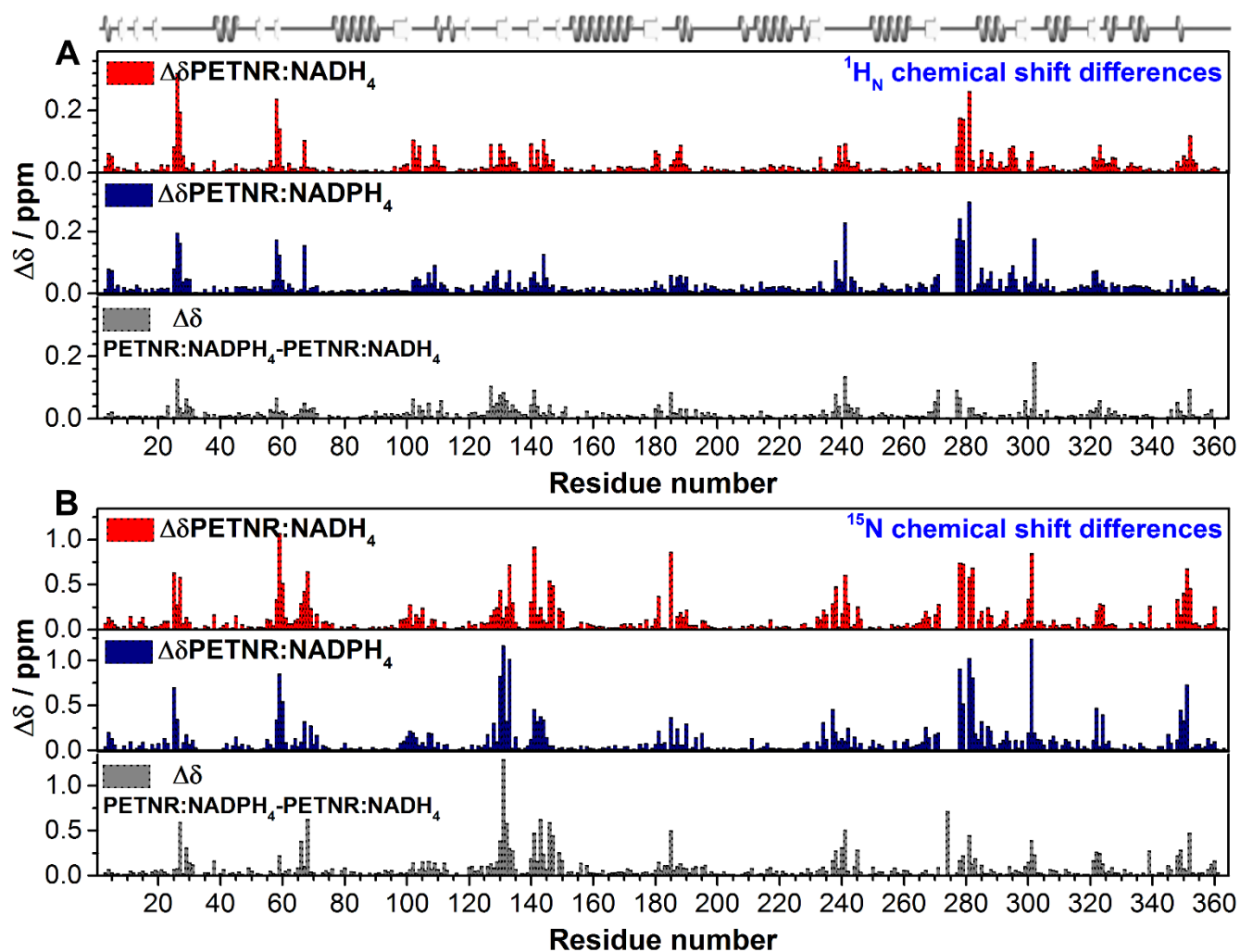
Figure S11. Histograms of (A) backbone amide proton (^1H_N) and (B) backbone amide nitrogen (^{15}N) residue-specific chemical shift changes that occur upon binding NADH$_4$ (red) and NADPH$_4$ (blue) to PETNR and the chemical shift differences between the PETNR−NAD(P)H$_4$ complexes (gray). The absolute chemical shift differences were calculated using the following equations: $\Delta\delta_X = [(\delta_X(\text{PETNR}) - \delta_X(\text{PETNR−NAD(P)H}_4))^2]^{1/2}$, where X = H$_N$ or N; $\Delta\delta_X = [(\delta_X(\text{PETNR−NADPH}_4) - \delta_X(\text{PETNR−NADH}_4))^2]^{1/2}$, where X = H$_N$ or N. The chemical shift assignments used for PETNR (holoenzyme) were previously deposited at BMRB (accession number 27224).[4]
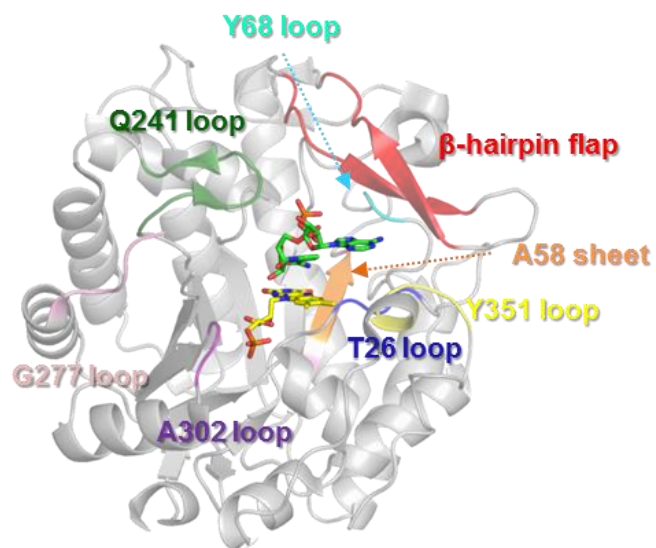
Figure S12. Structural representation of regions affected by NAD(P)H$_4$ binding to PETNR. The crystal structure of the PETNR–NADH$_4$ complex (PDB: 3KFT), with highlighted regions that are substantially affected by NAD(P)H$_4$ binding. The FMN cofactor is show as yellow sticks and the NADH$_4$ coenzyme analogue is shown as green sticks.
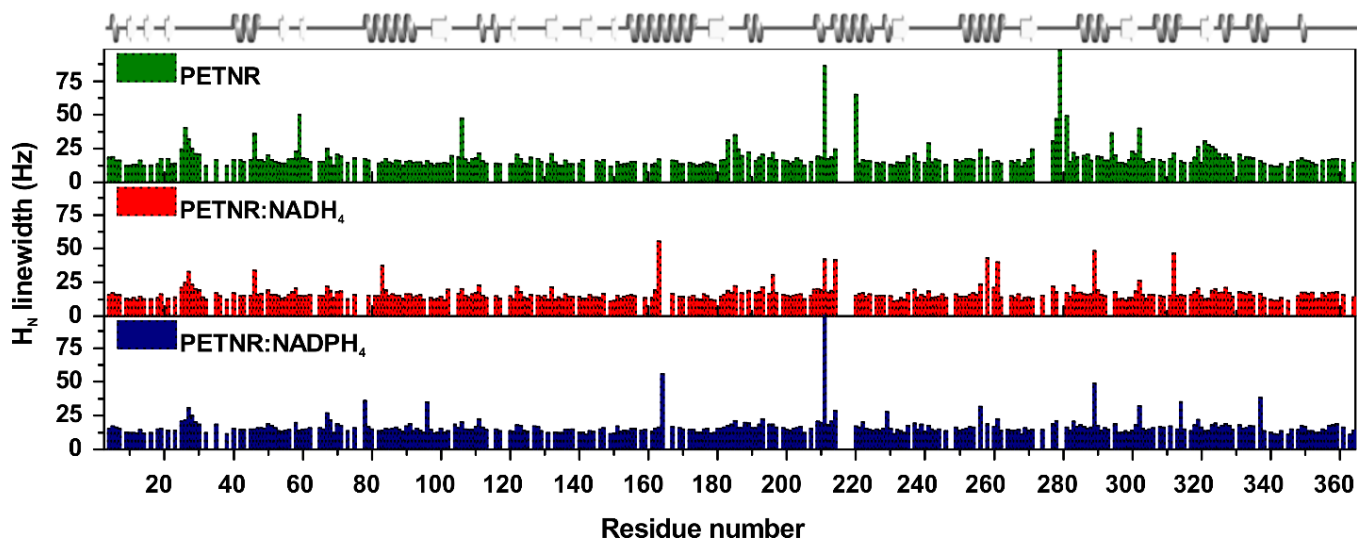
Figure S13. Distribution of ^{1}H line width values from ^{1}H-^{15}N TROSY spectra of PETNR and PETNR−NAD(P)H$_4$ complexes. The spectrum of each species was processed in an identical manner before analysis. Overlapped peaks were excluded from the data.
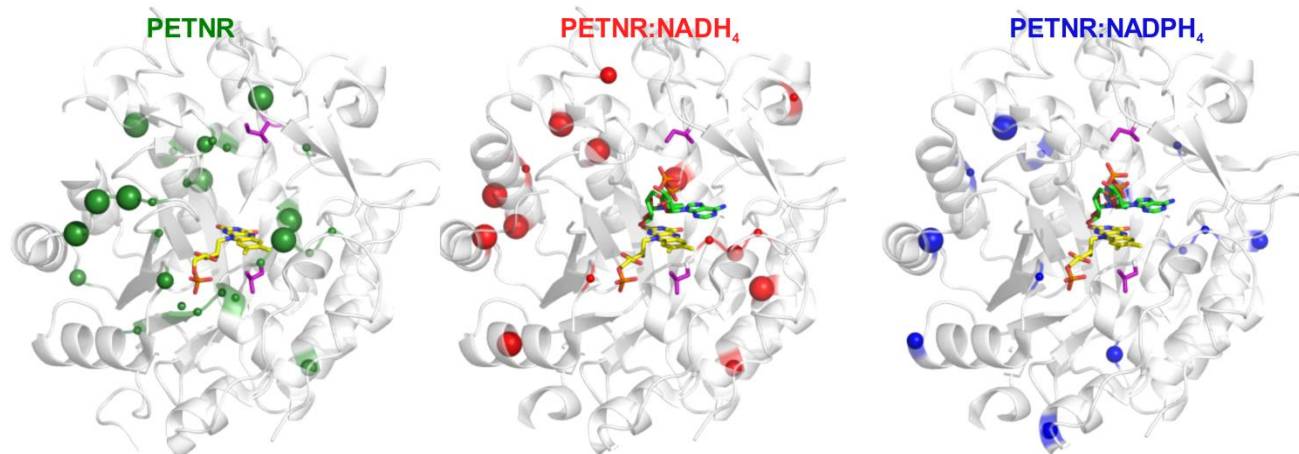
Figure S14. Line broadening analysis indicates regions affected by slow (μs-ms) dynamics in PETNR and the PETNR−NAD(P)H$_4$ complexes. Structural mapping of residues that exhibit line broadening depicted onto the crystal structure of PETNR (PDB:1H50) or PETNR−NADH$_4$ (PDB: 3KFT). The average line width and the standard deviation (σ) from the average for each residue-specific line width value were calculated (Figure S12). The residues that presented a ^{1}H line width value higher than the average value plus one standard deviation were considered broadened and are depicted as colored spheres at the Cα position. Three different sizes were used for the spheres, with the largest size depicting residues with significant broadening (values higher than average value plus $3 \times \sigma$).

REFERENCES

(1)   Pudney, C. R.; Hay, S.; Scrutton, N. S. Practical Aspects on the Use of Kinetic Isotope Effects as Probes of Flavoprotein Enzyme Mechanisms. *Methods Mol. Biol.* **2014**, *1146*, 161–175.

(2)   French, C. E.; Nicklin, S.; Bruce, N. C. Sequence and Properties of Pentaerythritol Tetranitrate Reductase from *Enterobacter Cloacae* PB2. *J. Bacteriol.* **1996**, *178*, 6623–6627.

(3)   Barna, T. M.; Khan, H.; Bruce, N. C.; Barsukov, I.; Scrutton, N. S.; Moody, P. C. E. Crystal Structure of Pentaerythritol Tetranitrate Reductase: "Flipped" Binding Geometries for Steroid Substrates in Different Redox States of the Enzyme. *J. Mol. Biol.* **2001**, *310*, 433–447.

(4)   Iorgu, A. I.; Baxter, N. J.; Cliff, M. J.; Waltho, J. P.; Hay, S.; Scrutton, N. S. ^{2}H, ^{15}N and ^{13}C Backbone Resonance Assignments of Pentaerythritol Tetranitrate Reductase from *Enterobacter Cloacae* PB2. *Biomol. NMR Assign.* **2018**, *12*, 79–83.

(5)   Winter, G. Xia2: An Expert System for Macromolecular Crystallography Data Reduction. *J. Appl. Crystallogr.* **2010**, *43*, 186–190.

(6)   McCoy, A. J.; Grosse-Kunstleve, R. W.; Adams, P. D.; Winn, M. D.; Storoni, L. C.; Read, R. J. Phaser Crystallographic Software. *J. Appl. Crystallogr.* **2007**, *40*, 658–674.

(7)   Emsley, P.; Lohkamp, B.; Scott, W. G.; Cowtan, K. Features and Development of Coot. *Acta Crystallogr. Sect. D Biol. Crystallogr.* **2010**, *66*, 486–501.

(8)   Afonine, P. V.; Grosse-Kunstleve, R. W.; Echols, N.; Headd, J. J.; Moriarty, N. W.; Mustyakimov, M.; Terwilliger, T. C.; Urzhumtsev, A.; Zwart, P. H.; Adams, P. D. Towards Automated Crystallographic Structure Refinement with Phenix.refine. *Acta Crystallogr. Sect. D Biol. Crystallogr.* **2012**, *68*, 352–367.

(9)   Chen, V. B.; Arendall, W. B.; Headd, J. J.; Keedy, D. A.; Immormino, R. M.; Kapral, G. J.; Murray, L. W.; Richardson, J. S.; Richardson, D. C. MolProbity: All-Atom Structure Validation for Macromolecular Crystallography. *Acta Crystallogr. Sect. D Biol. Crystallogr.* **2010**, *66*, 12–21.

(10)   Joosten, R. P.; Long, F.; Murshudov, G. N.; Perrakis, A. The *PDB_REDO* Server for Macromolecular Structure Model Optimization. *IUCrJ* **2014**, *1*, 213–220.

(11)   Pudney, C. R.; Hay, S.; Scrutton, N. S. Bipartite Recognition and Conformational Sampling Mechanisms for Hydride Transfer from Nicotinamide Coenzyme to FMN in Pentaerythritol Tetranitrate Reductase. *FEBS J.* **2009**, *276*, 4780–4789.

(12)   Markley, J. L.; Bax, A.; Arata, Y.; Hilbers, C. W.; Kaptein, R.; Sykes, B. D.; Wright, P. E.; Wüthrich, K. Recommendations for the Presentation of NMR Structures of Proteins and Nucleic Acids – IUPAC-IUBMB-IUPAB Inter-Union Task Group on the Standardization of Data Bases of Protein and Nucleic Acid Structures Determined by NMR Spectroscopy. *J. Biomol. NMR* **1998**, *12*, 1–23.

(13)   Gardner, K. H.; Kay, L. E. The Use of ^{2}H, ^{13}C, ^{15}N Multidimensional NMR to Study the Structure and Dynamics of Proteins. *Annu. Rev. Biophys. Biomol. Struct.* **1998**, *27*, 357–406.

(14)   Vranken, W. F.; Boucher, W.; Stevens, T. J.; Fogh, R. H.; Pajon, A.; Llinas, M.; Ulrich, E. L.; Markley, J. L.; Ionides, J.; Laue, E. D. The CCPN Data Model for NMR Spectroscopy: Development of a Software Pipeline. *Proteins Struct. Funct. Bioinforma.* **2005**, *59*, 687–696.